Laser and Particle Beams (2006), *24*, 283–290. Printed in the USA.

DOI: 10.1017/S0263034606060435

Experience of micro-heterogeneous target fabrication to study energy transport in plasma near critical density

A.M. KHALENKOV[1], N.G. BORISENKO[1], V.N. KONDRASHOV[2], Yu.A. MERKULIEV[1], J. LIMPOUCH[3], AND V.G. PIMENOV[4]

[1]Lebedev Physical Institute, Moscow, Russia
[2]Troitsk Institute for Innovation and Thermonuclear Research, Troitsk, Russia
[3]Czech Technical University in Prague, Prague, Czech Republic
[4]Zelinsky Institute of Organic Chemistry, Moscow, Russia

(RECEIVED 5 January 2005; ACCEPTED 20 February 2005)

Abstract

The experience of target fabrication with low-density and cluster heterogeneity is presented. Cluster plasma research is strongly dependent on target fabrication development and target structure characterization. Ten more target parameters should be measured for experiment interpreting in case of micro-heterogeneous plasma. Foam and foil targets, high-Z doped also, are produced and irradiated on the existing laser facilities. The density of 4.5 mg/cc cellulose triacetate in the form of regular three-dimensional polymer networks are achieved which is as low as plasma critical density for the third harmonic of iodine laser light. The possibilities of varying important target parameters, methods of their monitoring are discussed. Experiments with underdense foam targets with or without clusters irradiated on Prague Asterix Laser System (PALS) laser facility are analyzed preliminary for target optimization. Under-critical foams of varying structure (closed-cell foam or three-dimensional networks) and densities are reported for plasma experiments. Thermal and radiation transport in such targets are considered.

Keywords: Cluster target fabrication; Laser driven plasma; Low-density plastic foams; Thermal and radiation transport in plasma

1. INTRODUCTION

Doping of the targets material with high-Z elements for improving the resulting plasma characteristics and for diagnostic purposes is widely used in laser-plasma experiments. The admixed material can appear in the target either in atomic state or in the form of clusters—association of thousand of atoms. The resulting targets will have the clearly visible fluctuations of density and/or structure on microscopic scales while staying homogeneous on macroscopic scales (Borisenko *et al*., 1994). We call such targets micro-heterogeneous targets. They may produce plasma *different* both from dust plasma and from gas-jet cluster plasma.

The interaction processes of intense lasers with gas-jet clusters are currently studied experimentally and theoretically in many research groups (Kanapathipilliai, 2006; Mulser *et al*., 2005; Fukuda *et al*., 2004, Greschik & Kull, 2004; Shokri *et al*., 2004*a*, 2004*b*). The micro-heterogeneous (foam and cluster) targets can be used in the various laser experiments: (1) studying the corona region of irradiated target with volume absorption, (2) the conversion of visible light to X-rays (used in the indirect-drive hohlraum targets or in outer absorber-converter of the direct-drive targets) (Gus'kov & Merkuliev, 2001), (3) the experiments focused on studying the magnetic fields, generated in plasma and the possibilities of fields control in order to obtain more stable plasma via developing of the targets with given cluster distribution, (4) damping of Raleigh–Taylor (RT) and Richtmeyer–Meshkov (RM) instabilities (Grun *et al*., 1984; Fincke *et al*., 2005; Rudraiaah *et al*., 2004), (5) studying of the extremely non-ideal plasma, such as present in some astrophysical objects, for example, laboratory astrophysics applications (Remington, 2001), and (6) laser-cluster interaction can produce intense bursts of light harmonics, charged particles and neutrons as well as give birth to the magnetic fields and the vortices (Borisenko *et al*., 2003).

The laser experiment was published (Koch *et al*., 1995) aimed to reach the volume absorption in the under-critical polymer web-like structure (three-dimensional (3D) net-

Address correspondence and reprint requests to: N. G. Borisenko, Lebedev Physical Institute, 53 Leninsky pr., Moscow, 119991, Russia. E-mail: ngbor@sci.lebedev.ru

works) with the cell sizes of 10–15 micron. In the present work, we discuss the recently developed cellulose triacetate (TAC) targets of regular web-like structure, characterization before laser shot, and preliminary data illustrating laser interaction with such under-critical low-density and cluster foam targets obtained on Prague Asterix Laser System (PALS) facility in Prague (Limpough *et al*., 2004). The main results being processed are presented elsewhere.

2. TARGET APPROACH

In order to fulfill part of the above six tasks, a technology to produce low-density materials with open-cell structure (of the type of web-like 3D regular network), and with essential high-Z clusters concentration being developed during the past three years (Khalenkov *et al*., 2004). One of the problems was to obtain such under-critical materials with the average pore ranges 0.5–2 μm, 10–20 μm, and 50–100 μm. In targets, those could help to study and compare the processes of laser-light volume absorption in under-critical solids, the time periods of structured plasma homogenization, and the processes of energy transfer in such. Polymers were supposed to withstand thermal treatment up to 170–200 °C in order to allow DT-fuel filling when used in targets.

Most of low-density polymer materials are produced by gel structure formation from the solution with the subsequent drying. Introducing high (>10%) concentration of clusters influence, the gel formation process fundamentally. It proves possible only with high polymer concentration (2–3%) solutions. Such structures could be under-critical only for second and third harmonics of Nd-laser.

The main research is done for developed biopolymers and derivatives such as agar, cellulose ethers, and others as well as artificial materials of polyvinilformal, epoxy resin, and so on. Ultra dispersive powders of different metals (copper, nickel, silver) with the average particle diameters of 30–100 nm were used for metal loading. Finally, copper clusters were preferred because of their less chemical activity, although the surface still needs to be passivating before processing. With cellulose triacetate densities of 20 mg/cc at copper load of 35% the gelling process drops rapidly, so the enhanced densities of 3% polymer concentration become obligatory which result in foam densities of 40–50 mg/cc.

In order to investigate structure, density, and additives influence on the laser radiation absorption, and energy transport processes in structured plasma the targets of TAC and of agar, both with and without clusters, were fabricated.

The TAC foams were produced by a super-critical drying method, in which the alcohol in the polymer gel was substituted by liquid CO_2, with subsequent heating under the pressure to the critical point, where CO_2 changed from liquid state to the gaseous state without evaporation, and damaging the microstructure of web-like polymer. The ultra dispersive Cu powder with approximately 400 angstroms (40 nm) "clusters" is mixed with the solution of polymer, and distributed uniformly by the ultrasonic treatment before the gelation stage.

The agar foams were produced by a freeze-drying method, where the polymer solution is rapidly frozen and the solvent is removed by a vacuum drying process. The high-Z dopants if needed are also mixed with the polymer solution prior to gel formation. Scanning electron micrographs of the 4.5 mg/cc TAC target surface microstructure are shown in Figure 1.

For PALS experiment, two different foam types were prepared. The fine-structured micron-cell foams of cellulose triacetate (TAC, $C_{12}H_{16}O_8$) were used. The TAC foams

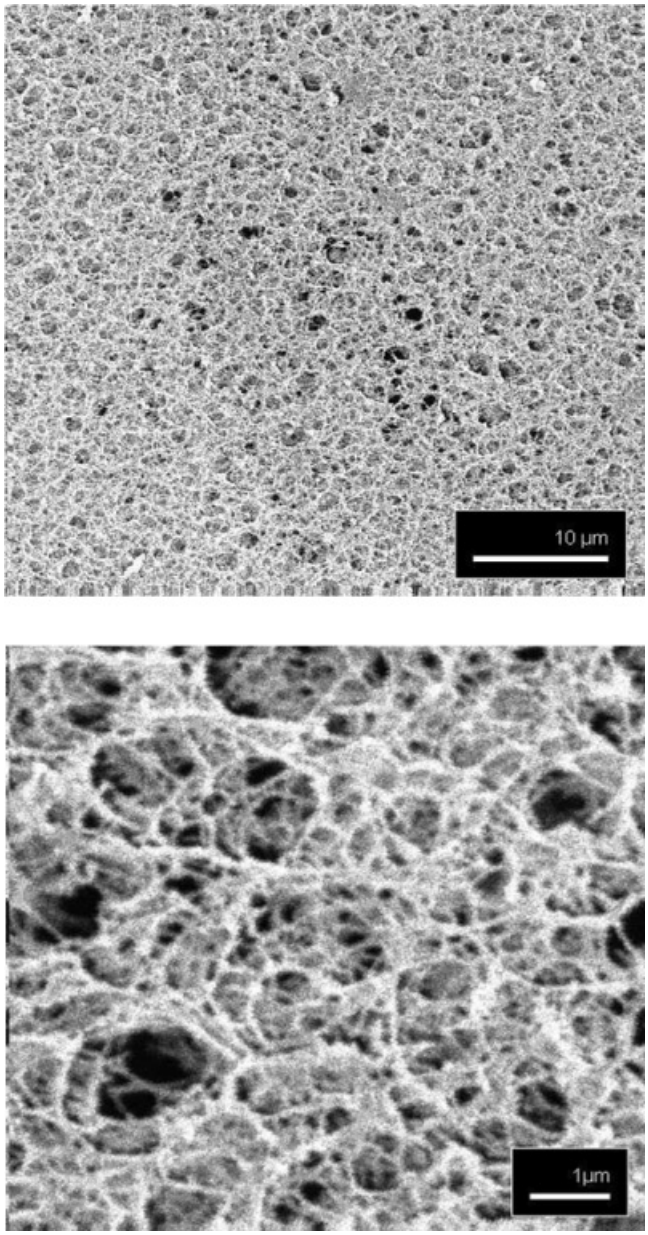

Fig. 1. SEM micrographs of 4.5 mg/cc cellulose triacetate foam with (**a**) 10 μm scale, (**b**) 1 μm scale.

https://doi.org/10.1017/S0263034606060435 Published online by Cambridge University Press

Table 1. *Targets for PALS experiment*

TAC (0.5–3 μm-size cells)				Agar (30–100 μm-size cells)			
	9.1mg/cc+9.9wt% Cu	9.1 mg/cc	4.5 mg/cc	20mg/cc	10mg/cc	5mg/cc	+50%SnO_2
***$Ne_{3\omega}$**	****0.53 $Ncr_{3\omega}$**	**0.54$Ncr_{3\omega}$**	**0.26$Ncr_{3\omega}$**	**1.2$Ncr_{3\omega}$**	**0.6$Ncr_{3\omega}$**	**0.3$Ncr_{3\omega}$**	**0.5÷0.7 $Ncr_{3\omega}$**
$Ne_{1\omega}$	4.76 $Ncr_{1\omega}$	4.8 $Ncr_{1\omega}$	2.34 $Ncr_{1\omega}$	10.7 $Ncr_{1\omega}$	5.3 $Ncr_{1\omega}$	2.7 $Ncr_{1\omega}$	4.5÷6.3 $Ncr_{1\omega}$
Foil 2 μm, foam thickness 380–480 μm				Foil 2 μm, foam thickness 200–600 μm			
Foil 5 μm, foam thickness 380–500 μm				Foil 5 μm, foam thickness 200–600 μm			

*Electron density in assumption of full ionization of the elements of the target material
**Critical plasma density for the appropriate harmonic—basic (1ω or third 3ω)

are optically transparent and characterized by highly uniform 3D network structure with $1 \div 2$ μm pores, 0.1 μm fibers with density of approximately 0.1 g/cc, small (<0.5%) density fluctuations on the focal-spot size area of 100×100 μm^2. Rougher agar–agar foams ($C_{12}H_{18}O_9$) with semi-closed cells up to 100 μm were used. The optically opaque foams with large closed and semi-closed pores of 30–100 μm diameters were less uniform in density (30%) on the focal-spot size area of 100×100 μm^2. Each foam type was done with high-Z load as well. The foams characteristics are presented in Table 1. In both cases, the doping of foam material with high-Z additives led to certain changing (roughening) of the microstructure for the same average density (see Fig. 2).

For the PALS experiment, the target was mounted in the washer of 8 mm outer diameter and 2.5 mm inner opening diameter with or without slit for X-ray streak camera. From the rear-side, all targets were covered by Al-foils of the

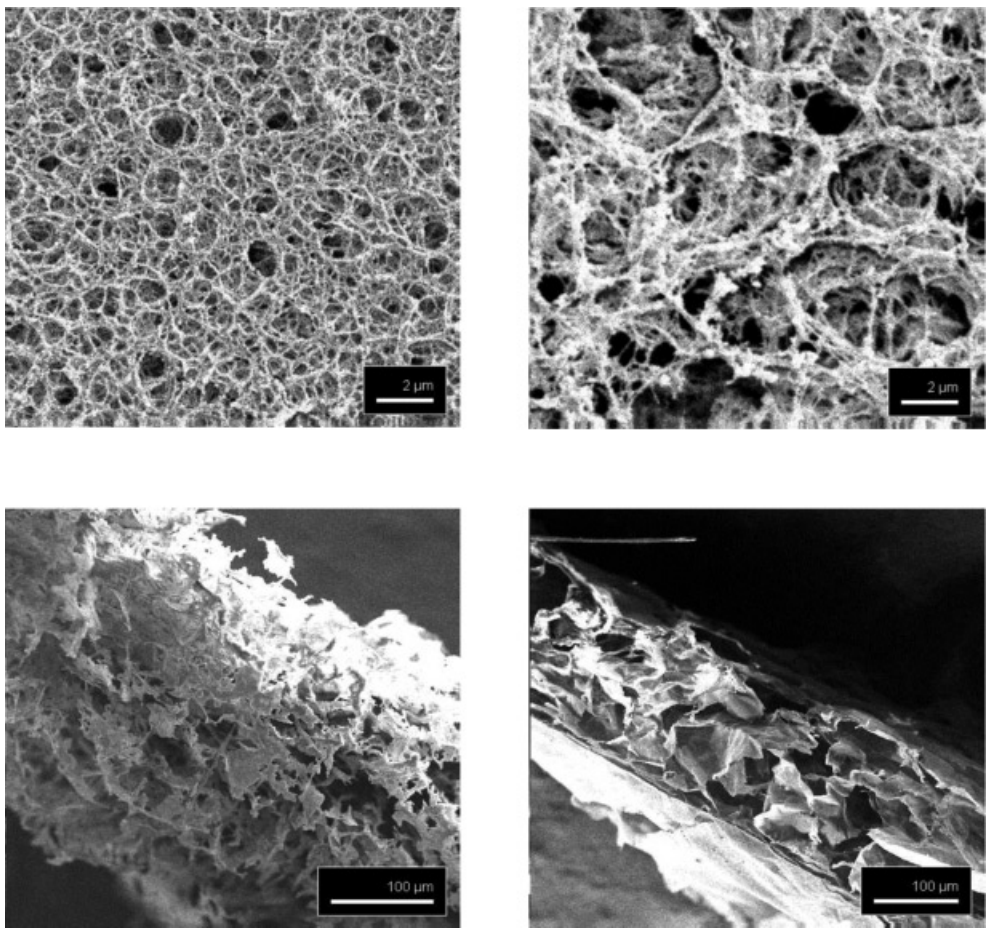

Fig. 2. Changing (roughening) of the microstructure of TAC foam in presence of Cu clusters and of metal-loaded agar. From left to right: TAC, $\rho = 9.1$ mg/cc 2 μm scale; TAC + Cu 9.9% wt., $\rho = 9.1$ mg/cc, 2-μm scale; Agar 10 mg/cc + SnO_2 10 mg/cc, 100-μm scale; Agar 20 mg/cc, 100-μm scale.

https://doi.org/10.1017/S0263034606060435 Published online by Cambridge University Press

thickness of 2 μm, 5 μm, 9 μm, or 15 μm. The inner opening of the washer was filled with TAC solution before gelation and drying process. The agar slices were cut from prefabricated disks and mounted inside the washers individually. The thicknesses of the targets were measured before each shot and varied from 200 μm to 600 μm for agar. For all TAC targets, the thicknesses ranged between 320 μm and 480 μm. For the sake of convenient theoretical modeling, special targets were done with two foils of Al (or Mylar + Al), separated by spacing equal to conventional foam layer thickness 380 μm or 180 μm.

To study how the target microstructures influence the results of the experiment, the characterization of the target proves to be not reducible to measuring only macroscopic parameters. Even more (up to 12 parameters) should be defined in presence of high-Z cluster dopant to the accuracy of units of percent. In practice, not all the parameters can be measured simultaneously, and with sufficient accuracy. Accuracy is the theoretical requirement to the measuring technique to be able to compare with simulation.

3. LASER EXPERIMENT

The goals of the experiment were: (1) Develop low-density layers of different structure (including 3D networks) and densities (down to 4mg/cc equivalent to 0.25 critical densities) with or without clusters. (2) Study laser interaction with targets of densities below and above critical, also in the presence of clusters. (3) Measure transport velocities for different cell sizes, and structures of low density material (foams, 3D networks). (4) Compare interaction of the first and the third laser light harmonics with low-density materials. (5) Study the processes of smoothing laser pulse inhomogenieties by coating target with foam of various thickness and density.

PALS were used for target irradiation (Jungwirth *et al*., 2001). The single-channel iodine laser provided irradiation either at first harmonic 1.315 μm wavelength or at third harmonic (0.438 μm), with maximum pulse energy 500 J, 350 ps pulse duration, focal spot of about 300 μm (minimal 70 μm), flux density on target surface about 10^{15} W/cm^2, beam intensity contrast $K > 10^7$, and laser radiation was at normal incidence on the target surface. The laser system is characterized by good shot-to-shot reproducibility and uniform spatial distribution of focal spot.

The diagnostic complex (see Fig. 3) for the present experiments consisted of optical and X-ray streak cameras, and three-frame shadowgraph/interferometry (Pisarczyk *et al*., 1994). The X-ray streak camera positioned in target plane was used to obtain the spatial and time-resolved pictures ($E > 1.4$ keV, 1.9 μm/pixel spatial resolution, 2 ps/pixel time resolution) of X-rays emitted from foam. The optical streak camera positioned normal to the rear-side of the target allowed to obtain the time sweep (11 ps/pixel time resolution) of optical luminescence of Al foil. Three-frame shadowgraphs were used to make the

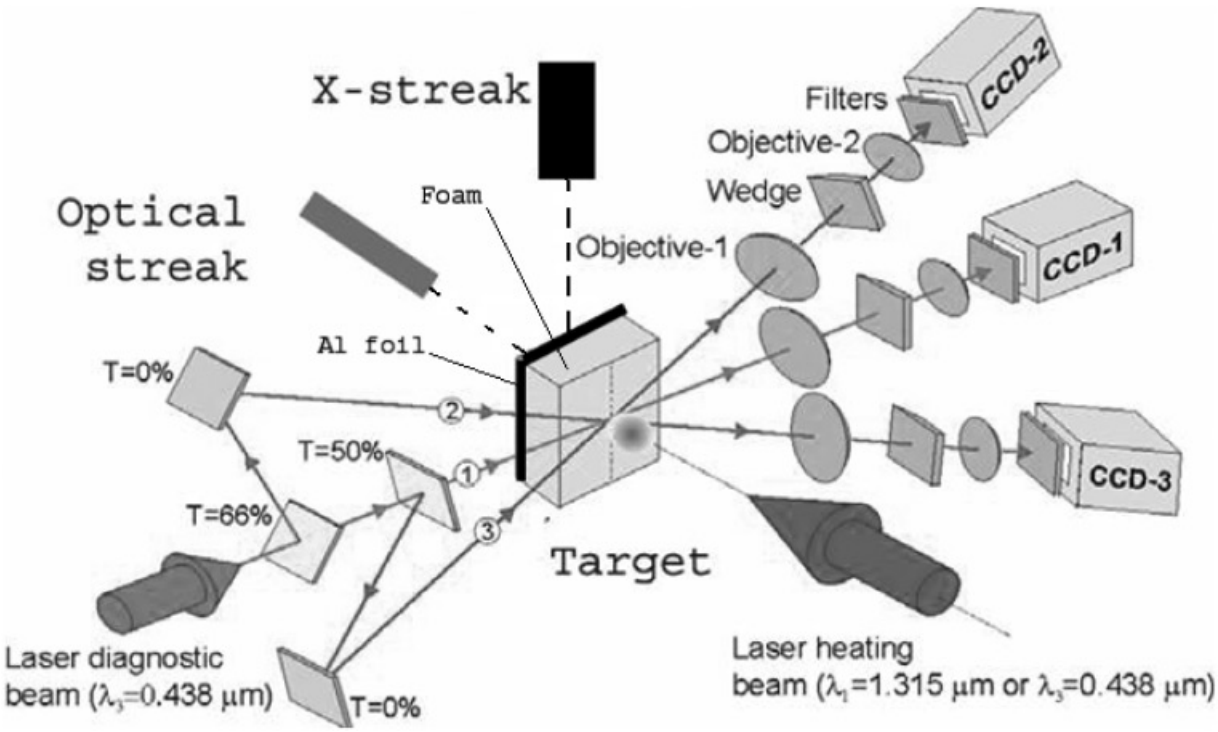

Fig. 3. Diagnostic complex of the PALS facility. X-streak camera in the plane of the target, optical streak camera situated normally to the rear side of the Al layer, CCD 1÷3 for three-frame interferometry. Laser radiation falls on the target surface at normal incidence.

https://doi.org/10.1017/S0263034606060435 Published online by Cambridge University Press

detailed pictures of foil expanding from the rear side of the target.

4. RESULTS

The primary experimental data consisted of time-resolved pictures of X-ray emission from the lateral side of the target and pictures of time-resolved optical self-emission of the rear-side of the Al foil complemented with three-frame shadowgraphs.

Typical data obtained from X-ray streak camera is shown in Figure 4. The starting position of Al-foil and the surface of the foam covering the foil are indicated by the horizontal lines (solid and dashed, respectively). Al-plasma formation is seen in the lower left part of the picture. We consider the fast radiation wave reaching the Al-foil surface at the moment when its luminescence starts. It is indicated by the small arrow, the bent giving the fast radiation velocity.

The second arrow in the middle position is the tangent to the outside contour of coronal plasma emitting region. This indicates the second velocity considered for visible X-ray emission front propagation in the beginning of laser-foam interaction. It is not constant in time. Slowing down of the X-ray front is withdrawn from the curvature of the lower boundary of emitting region.

The third dotted arrow is drawn as tangent to the brightest region witnessing the hottest front movement. It may be called slow "hydrothermal" wave. And optical emission from the rear-side of Al-foil appears no earlier than this hydrothermal wave provides energy transfer through foam and foil.

Intense expansion of corona is seen on the upper boundary of the image. The moment when it develops looks as if there are reflected radiation wave, providing additional heating-moving to the outside coronal region.

The arrows of the above mentioned transfer mechanisms are indicated for three targets (TAC 4.5 mg/cc, TAC 9.1 mg/cc, and TAC 9.1 mg/cc with Cu clusters 9.9% wt.) and presented in Figure 5. The slowing down of corresponding velocities with density growth (still remaining under-critical!) and changes with clusters added are illustrated qualitatively.

The examples of optical streak image for TAC foams under 3ω (upper row) and 1ω (lower row) irradiation are shown in Figure 6, time is increasing at the bottom, the full height of the picture corresponds to 5.68 ns. Five micrometers Al foil covers the rear-side of the target in all shots. From left to right, the foams on the foil in each row are, respectively, TAC 4.5 mg/cc, TAC 9.1 mg/cc, and TAC 9.1 mg/cc with 9.9 wt% Cu content. For 3ω, the time fiducial mark (spot in the upper left corner of each frame) comes simultaneously with the maximum of laser pulse, except for the upper left shot, where fiducial mark were shifted 3 ns after the maximum. For 1ω, time fiducial mark is shifted 3 ns for each shot (comes later after the maximum). It is easily seen that the optical self-emission for 1ω appeared much later compared to 3ω experiments.

Such time delays are present for every density, all three being sub-critical for 3ω, and above critical density for the main wavelength. The weak emission of preheated Al is detected practically simultaneously with the coming maximum of the laser pulse for 3ω and is almost undetectable for

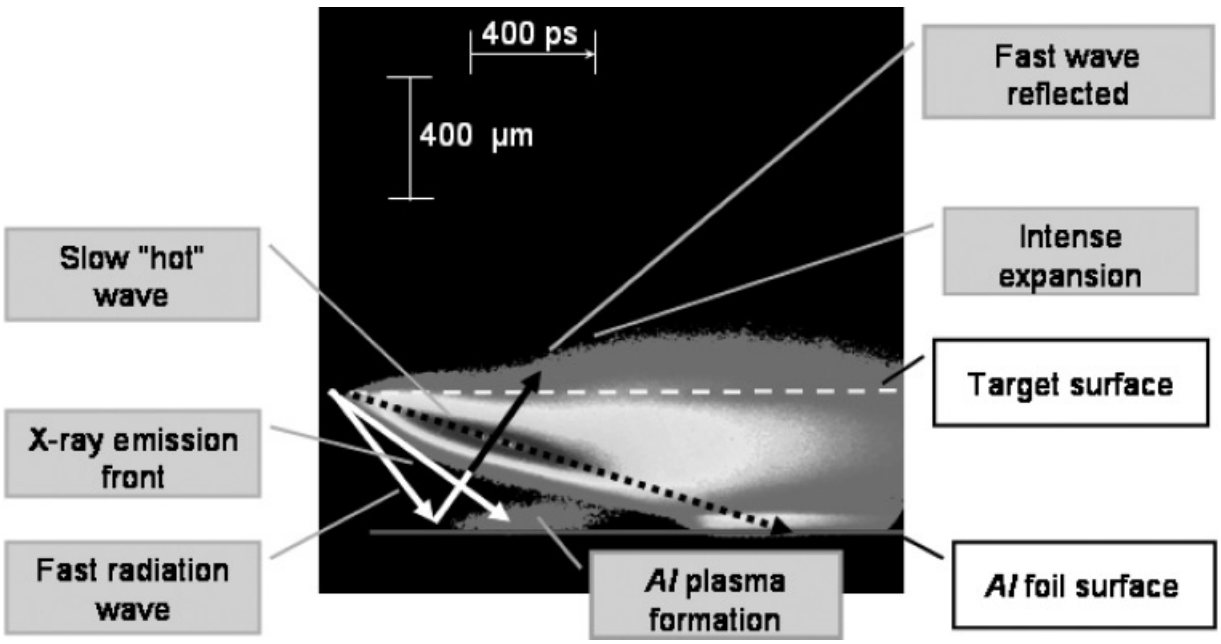

Fig. 4. X-ray streak-camera image of hot plasma behavior, when formed from foam and Al-layer target. Laser is incident from above. Time is increasing to the right. Shot # 28204, TAC 4.5 mg/cm^3, 3ω, E = 157 J, Al 5 μm. Scale is given by the bars.

https://doi.org/10.1017/S0263034606060435 Published online by Cambridge University Press

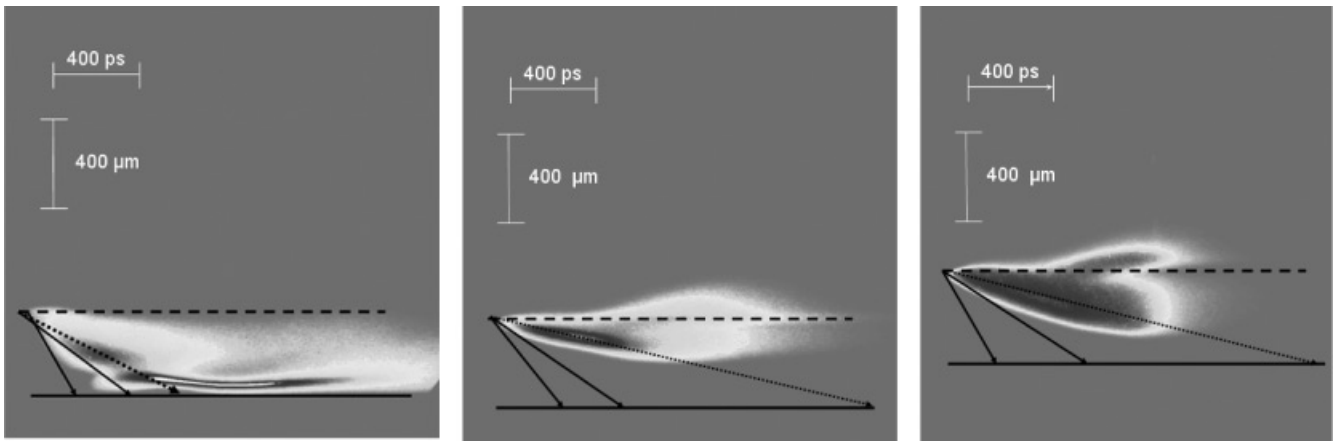

Fig. 5. The transfer mechanisms for three different targets under 3ω irradiation. From left to right: TAC 4.5 mg/cc (shot # 28233, E_l = 164 J), TAC 9.1 mg/cc (shot # 28207, E_l = 157 J) and TAC 9.1 mg/cc with Cu clusters 9.9% wt. (shot # 28211, E_l = 158 J). Foam thicknesses are about 400 μm in all shots, Al foil 5 μm. Time increase to the right, scale is given by the bars. Laser light is incident from above, the dotted horizontal line corresponds to the foam surface, and solid horizontal line corresponds to Al foil surface.

1ω. The strong emission caused by heat wave arrival on Al rear-side has performed time-delay depending on target foam-density and on presence of clusters in it.

The time period between X-ray radiation (of E > 1.4 keV) vanishing and starting of strong optical self-emission of Al rear-side is illustrated in Figure 7. Time is increasing to the right; the scale is given by the bars. For reference, the shape of laser pulse in appropriate time scale is shown in the upper left corner of the picture. Specific "two-tail" X-ray streak images are characteristic for TAC foams doped with Cu clusters.

5. DISCUSSION

Numerous technology research experiments proved that introducing clusters inside the low-density structures enhance the minimum reached density for the chosen composition almost by an order of magnitude. If similar low-density structures are needed with and without clusters, it could be possible only for densities exceeding 5 mg/cc. Thus, introducing 10 wt% Cu into the TAC 3D polymer network of 9.1 mg/cc density can be realized without drastic structure change. So targets with such "foams"

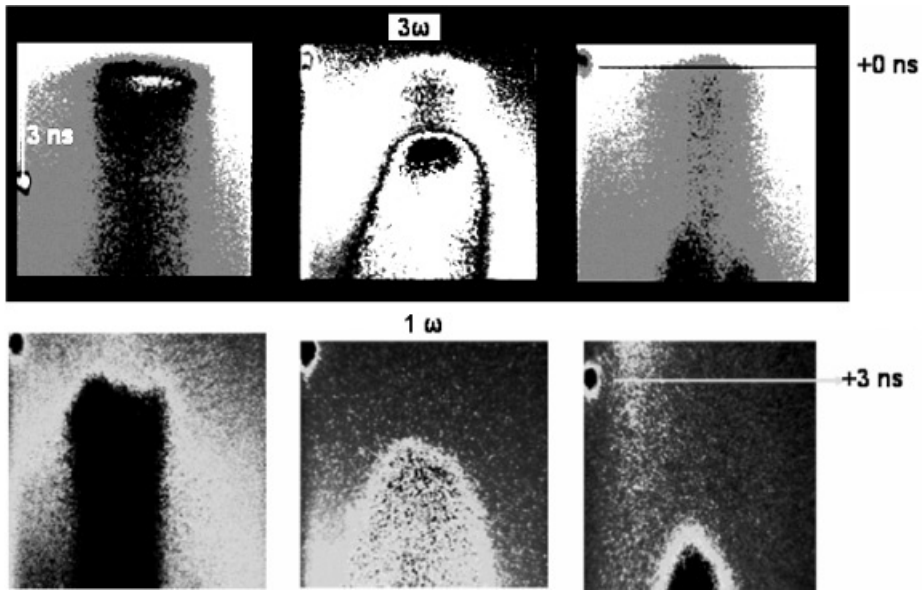

Fig. 6. Optical streak-camera data for six laser shots. 3 TAC foams (4.5 mg/cc, 9.1 mg/cc and 9.1 mg/cc with 9.9 wt% Cu) with 5 μm Al foil on the rear-side for 3ω irradiation (upper row) and 1ω (lower row) irradiation. Laser energy is the same ($\approx$ 170 J) for all shots. Time fiducial mark is 3-ns shifted (comes later after the pulse maximum) for 1ω and is not shifted for 3ω.

https://doi.org/10.1017/S0263034606060435 Published online by Cambridge University Press

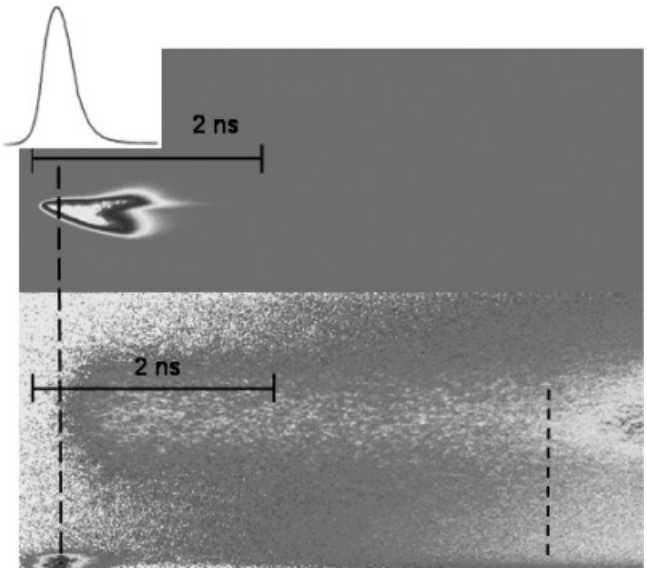

Fig. 7. The time delay between X-ray radiation vanishing and starting of optical self-emission of Al rear-side. Shot #28213, TAC + Cu 9.9%, $\rho = 9.1$ mg/cm^3, 3ω.

allow for comparative laser experiments with and without clusters.

High-Z additives in the foam change essentially the near-critical plasma behavior. In spite of almost equal mass density and electron density, the homogenization process slows down and heating wave arrival at the rear-side of Al-foil happens later than in the foam without clusters.

The technique developed to manufacture the 3D network can produce relatively smooth surface, so shot-to-shot reproducibility in experimental corona study is better than for rougher foams (of the type of agar or polystyrene). Technology to produce 3D networks of cellulose triacetate with clusters (TAC + clusters) is capable to obtain the fibers of the structure to be underdense themselves, fiber density being around 0.1 g/cc. Such tiny fiber structure can perform similarly to gaseous clusters under picosecond or femtosecond laser pulse irradiation. The additives other than Cu and Mo are possible as well, for example Au, Ag, and Ni.

Almost identical spatial structures with different cluster sizes were achieved. So the influence of cluster sizes in the range of 5–100 nm can be studied as regards energy transfer in such media.

The present plasma experiment with under-critical polymer target showed that laser light is absorbed near the boundary of low-density layer. "Fast wave" corresponds to the initial heating and homogenization of low-density material by hard X-rays. At foam transformation into homogeneous plasma the energy transfer process slows down. Further, it results in Al ablating into underdense region thus causing the diminished radiation transfer rate in highly ionized plasma.

"X-ray emission front" corresponds to the propagation of soft X-rays in partly homogenized plasma and also causes the intensive Al ablation. Even in the foam soft X-rays have fewer paths than the hard ones.

Hot front velocity is slower "hydrothermal" velocity of mass and heat transfer, and is responsible for the second bright maximum in Al emission. Different transfer processes interplay could be responsible for the outward foam boundary shape. "Hydrothermal" velocity is in reasonable agreement with the data of Batani *et al*. (2002) on flat target irradiated with soft X-rays. "X-ray emission front" and "slow hot wave" velocities measured are in reasonable agreement with the data of Koch *et al*. (1995) from experiments with agar targets of densities and structure similar to ours. In experiments with clusters, there exists the essential time-delay in the optical signal appearing from the rear-side of Al-foil on the foam. This might be connected, first, with the radiation cooling of rarified plasma, and, second, with strong flux of hard X-ray radiation from "foam-induced" plasma onto the surface of Al. The latter transfers into Al-plasma flux encountering the main plasma stream and cools hot plasma also. The "two-tail" structure of the end of the sweep from X-ray streak camera might be connected with Al-caused densification wave escape to the critical surface and its burst as a thin shell.

6. CONCLUSION

Materials and targets are developed and used for laser experiment with foam smoothing and transport studies. Densities as low as $0.25N_{cr}$ are realized for laser targets, absolute density for 3D networks being down to 4.5 mg/cc (optically transparent). Open cells of 1 μm and 30 μm are demonstrated in a variety of materials. Layers of foams with high-Z load were realized on the target surface including either uniform spread or cluster dispersion up to 30% wt. For adequate modeling and experimental results interpretation each target may need up to 12 parameters measured for proper characterization.

Laser experiments with the layered target of two relatively thin "foam" and Al-foil layers unveiled that the results could be understood at simultaneous accounting of hard and soft X-rays interaction with either layer. To explain essential optical signal delay from the rear surface of Al-foil needs the detailed simulation taking into consideration the radiation cooling of plasma.

ACKNOWLEDGMENTS

Part of this work was supported by the RFBR project # 06-02-17526. The authors gratefully acknowledge the heads and staff of Prague Asterix Laser facility for organizing and performing the experiments (M. Kalal, E. Krousky, K. Masek, M. Pfeifer, K. Rohlena, M. Sinor, J. Ullschmied, B. Skala, and J. Straka), A. Kasperczuk, T. Pisarczyk, and P. Pisarczyk for providing three-frame interferometry, S. F. Medovshikov for agar foams, W. Nazarov

for TMPTA targets, N. N. Demchenko, and S. Yu. Gus'kov for guidance and useful discussions, O. Renner for spectroscopic experiment data and discussion, A. I. Gromov for agar mounting and foil characterization, I. V. Akimova for SEM, and all other participants of the third year of INTAS project # 2001-0572.

REFERENCES

Batani, D., Desai, Lower., Th., Hall, T.A., Nazarov, W., Koenig, M. & Benuzzi-Mounaix, A. (2002). Interaction of soft-x-ray thermal radiation with foam-layered targets. *Phys. Rev. E*, **65**, 066404.

Borisenko, N.G., Akunets, A.A., Bushuev, V.S., Dorogotovtsev, V.M. & Merkuliev, Yu.A. (2003). Motivation and fabrication methods for inertial confinement fusion energy targets. *Laser Part. Beams* **21**, 505–509.

Borisenko, N.G., Merkuliev, Yu. A. & Gromov, A.I. (1994). Microheterogeneous targets—a new challenge in technology, plasma physics, and laser interaction with matter. *J. Moscow Phys. Soc* **4**, 47–73.

Fincke, J.R., Lanier, N.E., Batha, S.H., Hueckstaedt, R.M., Magelssen, G.R., Rothman, S.D., Parker, K.W. & Horsfield, C. (2005). Effect of convergence on growth of the Richtmyer-Meshkov instability. *Laser Part. Beams* **23**, 21–25.

Fukuda, Y., Akahane, Y., Aoyama, M., Inoue, N., Ueda, H., Kishimoto, Y., Yamakawa, K., Faenov, A.Y., Magunov, A.I., Pikuz, T.A., Skobelev, I.Y., Abdallah, J., Csanak, G., Boldarev, A.S. & Gasilov, V.A. (2004). Generation of X rays and energetic ions from superintense laser irradiation of micron-sized Ar clusters. *Laser Part. Beams* **22**, 215–220.

Greschik, F. & Kull, H. (2004). Two-dimensional PIC simulation of atomic clusters in intense laser fields. *Laser Part. Beams* **22**, 137–145.

Grun, J., Emery, M.H. & Kacenjar, S. (1984). Observation of the Rayleigh-Taylor instability in ablatively accelerated foils. *Phys. Rev. Lett*. **53**, 1352–1355.

Gus'kov, S. Yu. & Merkuliev, Yu.A. (2001). Low-density absorber-converter of laser fusion targets for direct irradiation. *Quant. Electron* **31**, 311–317.

Jungwirth, K., Cejnarova, A., Juha. L., Kralicova, B., Krasa, J., Krousky, E., Krupickova, P., Laska, L., Masek, K., Mocek, T., Pfeifer, M., Prag A., Renner, O., Rohlena, K., Rus, B., Skala, J., Straka, P. & Ullschmied, J. (2001). The Prague Asterix Laser System. *Phys. Plasmas* **8**, 2495–2501.

Kanapathipilliai, M. (2006). Nonlinear absorption of ultra short laser pulses by clusters. *Laser Part. Beams* **24**, 9–14.

Khalenkov, A.M., Borisenko, N.G., Erokhin, A.A., Fedotov, S.I., Merkuliev, Yu. A., Osipov, M.V., Pimenov, V.G., Puzyrev, V.N., Starodub, A.N., Studenov, V.B. & Yakushev O.F. (2004). Cluster targets and experiments on KANAL-2 laser installation. *Proc. 28th European Conference on Laser Interaction with Matter*, pp. 277–282, Frascati, Roma: R.C. Enea.

Koch, J.A., Estabrook, K.G., Bauer, J.D., Back, C.A., Rubenchik, A.M., Hsieh, E.J., Cook, R.C., Macgowan, B.J., Moody, J.D., Moreno, J.C., Kalantar, D. & Lee, R.W. (1995). Time-resolved x-ray imaging of high-power laser-irradiated underdense silica aerogels and agar foams. *Phys. Plasmas* **2**, 3820–3831.

Limpough, J., Demchenko, N.N., Gus'kov, S.Yu., Kalal, M., Kasperczuk, A., Kondrashov, V.N., Krousky, E., Masek, K., Pizarczyk, P., Pizarczyk, T. & Rozanov, V.B. (2004). Laser interaction with plastic foam—metallic foil layered targets. *Plasma Phys. Cont. Fusion* **46**, 1831–1841.

Mulser, P., Kanapathipilliai, M. & Hoffmann, D.H.H. (2005). Two very efficient nonlinear laser absorption mechanisms in clusters. *Phys. Rev. Lett.* **95**, 103401.

Pisarczyk, T., Arendzikowski, R., Parys, P. & Patron, Z. (1994). Polari-interferometer with automatic images processing for laser plasma diagnostics. *Laser Part. Beams* **12**, 549–562.

Remington, B.A. (2001). High energy density astrophysics in the laboratory. *Proc. Inertial Fusion Sciences and Applications*, pp. 1003–1029, Osaka, Japan: Elsevier.

Rudraiaah, N., Krishnamurthy, B.S., Jalaja, A.S. & Desai, T. (2004). Effect of a magnetic field on the growth rate of the Rayleigh-Taylor instability of a laser-accelerated thin ablative surface. *Laser Part. Beams* **22**, 29–33.

Shokri, B., Niknam, A.R. & Krainov, V. (2004*a*). Cluster structure ellects on the interaction of an ultrashort intense laser field with large clusters. *Laser Part. Beams* **22**, 13–18.

Shokri, B., Niknam, A.R. & Smirnov, M. (2004*b*). Ionization processes in the ultrashort, intense laser field interaction with large clusters. *Laser Part. Beams* **22**, 45–50.